Published in final edited form as:
Nat Cell Biol. 2013 March ; 15(3): 249–260. doi:10.1038/ncb2679.

Spatial regulation of VEGF receptor endocytosis in angiogenesis

Masanori Nakayama[1,2], **Akiko Nakayama**[1], **Max van Lessen**[1], **Hiroyuki Yamamoto**[1], **Sarah Hoffmann**[1], **Hannes C.A. Drexler**[3], **Norimichi Itoh**[4], **Tomonori Hirose**[5], **Georg Breier**[6], **Dietmar Vestweber**[7], **Jonathan A. Cooper**[8], **Shigeo Ohno**[5], **Kozo Kaibuchi**[4], and **Ralf H. Adams**[1,2]

[1]Max-Planck-Institute for Molecular Biomedicine, Department of Tissue Morphogenesis, and University of Muenster, Faculty of Medicine, Muenster, Germany

[3]Max-Planck-Institute for Molecular Biomedicine, Bioanalytical Mass Spectrometry Facility, Muenster, Germany

[4]Department of Cell Pharmacology, Nagoya University Graduate School of Medicine, Nagoya, Japan

[5]Department of Molecular Biology, Yokohama City University School of Medicine, Yokohama, Japan

[6]Institute of Pathology, Medical Faculty Carl Gustav Carus, Dresden University of Technology, Dresden, Germany

[7]Max-Planck-Institute for Molecular Biomedicine, Department of Vascular Cell Biology, Muenster, Germany

[8]Fred Hutchinson Cancer Research Center, Seattle, USA

Abstract

Activities as diverse as migration, proliferation and patterning occur simultaneously and in a coordinated fashion during tissue morphogenesis. In the growing vasculature, the formation of motile, invasive and filopodia-carrying endothelial sprouts is balanced with the stabilisation of blood-transporting vessels. Here, we show that sprouting endothelial cells in the retina have high rates of VEGF uptake, VEGF receptor endocytosis and turnover. These internalisation processes are opposed by atypical protein kinase C activity in more stable and mature vessels. aPKC phosphorylates Dab2, a clathrin-associated sorting protein that, together with the transmembrane protein ephrin-B2 and the cell polarity regulator PAR-3, enables VEGF receptor endocytosis and downstream signal transduction. Accordingly, VEGF receptor internalisation and the angiogenic growth of vascular beds are defective in loss-of-function mice lacking key components of this regulatory pathway. Our work uncovers how vessel growth is dynamically controlled by local VEGFR endocytosis and the activity of cell polarity proteins.

[2]Authors for correspondence: Ralf H. Adams, ralf.adams@mpi-muenster.mpg.de; Phone: +49 251 70365 410; Fax: +49 251 70365 499, Masanori Nakayama, mnakaya@gwdg.de; Phone: +49 251 70365 427; Fax: +49 251 70365 499, Department of Tissue Morphogenesis, Max-Planck-Institute for Molecular, Biomedicine and University of Muenster, D-48149 Muenster, Germany.

Author Contributions

M.N., K.K. and R.H.A. designed the study. M.N., H.Y., H.D., and N.I. performed the identification of ephrin-B2 interacting proteins. M.V.L purified PAR-3 antibodies and GST-fusion proteins. T.H., S.O., G.B. D.V., and J.C. generated mouse mutants or lines. All other experiments have performed by M.N. A.N. and S.H.; M.N. and R.H.A. wrote the manuscript.

The authors declare that they have no competing financial interests.

Introduction

The biological activity of growth factor receptors is tightly controlled during growth and patterning processes. While internalisation is often seen as a means of terminating signals or degrading receptors, it can also generate qualitatively or quantitatively distinct signalling responses[1–3]. Consequently, the positive or negative regulation of endocytosis might facilitate specialized biological activities of certain cells or cell groups within a larger population, as they are frequently seen in morphogenesis[4]. In the angiogenic vasculature, sprouting involves the specialisation of endothelial tip cells, which are highly motile and invasive, and extend filopodia to detect tissue-derived cues such as VEGF growth factors. These ligands (primarily VEGF-A and VEGF-C) trigger the homo- or heterodimerisation of their cognate endothelial receptors (VEGFR2/Flk1 and VEGFR3/Flt4, respectively) and thereby activate downstream signal transduction cascades that control sprouting and proliferation[5–7]. Tip cells are thought to have the highest levels of VEGF receptor signalling because they lead sprouts and might therefore encounter higher ligand concentrations than trailing stalk cells. The latter form the sprout base, maintain a lumenised connection to the existing vasculature and lack long filopodia. Tip and stalk cell behaviours are presumably not fixed and rather reflect transient, interconvertible phenotypes and constant competition of endothelial cells (ECs) for the tip position[6,8]. This process involves the Notch pathway, which is thought to down-regulate VEGF receptor expression and is therefore presumably less active in tip cells[9–11]. Another cell contact-dependent signalling molecule, the Eph receptor ligand ephrin-B2 (encoded by the *Efnb2* gene), promotes the invasive behaviour of ECs and is required for normal VEGF receptor endocytosis and signalling[12–14].

Physiological angiogenesis also involves the gradual conversion of growing vessels into a stable and mature tubular network, in which ECs are increasingly quiescent, display a phalanx-like morphology and are devoid of VEGF-induced activities such as filopodia extension or proliferation[15]. The postnatal vascularisation of the retina in the mouse is an excellent model system for angiogenic sprouting and maturation, because sequentially occurring processes are spatially separated and can be imaged at high resolution[16]. Tip and stalk cell-containing sprouts can be found at the peripheral edge of the growing vascular plexus next to VEGF-producing tissue regions, whereas the previously established, more mature vessels are located in the central retina.

Here, we show that angiogenesis is controlled by spatially regulated endothelial endocytosis. We identify Disabled 2 (Dab2), a clathrin-associated sorting protein (CLASP)[17], and the cell polarity protein PAR-3 as interaction partners of ephrin-B2 and VEGF receptors. These proteins mediate VEGF receptor endocytosis, which is negatively regulated by atypical protein kinase C (aPKC), another component of the PAR polarity complex. aPKC phosphorylates Dab2 and reduces the interaction between the CLASP and its cargo. We propose that spatially controlled activity of aPKC, which is high in established vessels but low in endothelial sprouts, critically contributes to important regional differences in VEGF receptor endocytosis, turnover and signalling.

Results

Vessel beds exhibit spatial differences in VEGF receptor turnover

Previous work has provided evidence for high VEGF receptor transcript levels in the ECs at the peripheral edge (angiogenic front) of the growing retinal vasculature, which is consistent with models linking VEGF gradients to strong VEGF receptor expression, the activation of endothelial sprouting and the induction of filopodia-extending tip cells[16,18]. However, VEGFR2 and VEGFR3 immunostaining of the retinal vasculature at postnatal day 6 (P6) did not selectively label sprouting ECs. Anti-VEGFR3 signals showed the previously published

differences between arteries and veins (Fig. 1a, b)[19], but were not predominantly associated with vessel sprouts (Fig. 1a; Supplementary Fig. 1a). Even more surprisingly, immunosignals for the cytoplasmic region of VEGFR2 were almost undetectable in angiogenic sprouts, whereas comparably strong staining labelled the more established vasculature of the central retina (Fig. 1a, d). Confirming the specificity of these patterns, endothelial anti-VEGFR2 signal was absent in the retinal vasculature of EC-specific and inducible VEGFR2 (*Flk1*$^{i\Delta EC}$) loss-of-function mice (Fig. 1a). *Flk1*$^{i\Delta EC}$ vessels also displayed weaker signals for VEGFR3, which is consistent with previous reports placing VEGFR2 activity upstream of VEGFR3 expression[19,20].

We speculated that the surprisingly weak VEGFR2 immunoreactivity in sprouts might reflect rapid local turnover and, accordingly, low steady-state levels of this receptor. As previous reports have suggested that VEGFR2 in cultured cells can be degraded through proteasome as well as lysosome-dependent pathways[21–23], we intraocularly injected the proteasome inhibitors MG132 or MG115, the lysosome inhibitor Chloroquine, or MiTMAB and Dynasore, which are cell-permeable inhibitors of dynamin and endocytosis, into P6 pups. At 2 hours after injection, VEGFR2 and VEGFR3 protein levels were strongly increased in angiogenic sprouts, whereas immunosignals were significantly less enhanced in the vasculature of the central retina (Fig. 1b–d; Supplementary Fig. 1a, b). Indicating that this upregulation required new protein synthesis, no significant increase in VEGFR2 and VEGFR3 immunosignals were seen when proteasome inhibitors were co-administered with cycloheximide, a general inhibitor of protein translation (Fig. 1c, d; Supplementary Fig. 1b). As even short-term inhibition of protein degradation might lead to the stabilisation of Hypoxia-inducible factor, a key regulator of VEGF expression, and thereby to potential indirect effects, we also validated that *Flk1/Vegfr2* and *Flt4/Vegfr3* transcript levels were not significantly altered in inhibitor-injected pups (Fig. 1e).

As the data above suggested rapid turnover (i.e., degradation and new synthesis) of VEGF receptors at the angiogenic growth front, we next wanted to examine whether this activity was exclusively controlled by local differences in the availability of VEGF growth factors. To visualize the spatial pattern of internalisation processes, Alexa dye-coupled human VEGF-A (165 isoform) was administered by intraocular injection. From 45 minutes after injection onwards, accumulation of the labelled growth factor was observed in retinal ECs (Fig. 2a; Supplementary Fig. 1c). Strongly arguing that these signals corresponded to internalised VEGF, Alexa-labelled spots partially co-localised with EEA1, a marker of early endosomes, were frequently found in perinuclear localisation, and were strongly reduced in samples in which endocytosis had been blocked by dynamin inhibition (Fig. 2a; Supplementary Fig. 1d). Confirming that the uptake of Alexa dye-coupled VEGF-A was largely mediated by VEGFR2, signals in the vasculature were profoundly diminished in *Flk1*$^{i\Delta EC}$ vessels (Fig. 2b). Thus, spots of dye-labelled VEGF-A corresponded primarily to receptor- and dynamin-dependent internalisation of the ligand, as one would expect for clathrin-mediated endocytosis of ligand-receptor complexes. Next, we examined the spatial distribution of the exogenous and therefore uniformly provided Alexa dye-coupled growth factors. At 10 minutes after intraocular injection, fluorescent VEGF-A and VEGF-C were widely distributed throughout the central and peripheral retina (Supplementary Fig. 2a, b). In contrast, at 2 hours after injection, VEGF-A or VEGF-C spots were predominantly associated with ECs at the angiogenic front and only much weaker signals were visible in the central plexus (Fig. 2c; see Figure 5f and 7c for statistical analysis). Arguing against a major influence of matrix-binding motifs in the 165 isoform of VEGF-A in this distribution pattern, injection of the shorter 121 isoform also preferentially labelled ECs at the angiogenic front (Supplementary Fig. 2c). The sum of these results indicates previously unappreciated spatial differences in VEGF/VEGF receptor internalisation even when growth factors were presented uniformly and not in gradients or other patterns.

PAR-3 and Dab2 associate with VEGFRs and ephrin-B2

Previous work has shown that the Eph receptor ligand and transmembrane protein ephrin-B2 is an important regulator of VEGF receptor endocytosis and downstream signalling[12,13]. To gain further insight into the underlying molecular mechanism, we isolated interaction partners of the cytoplasmic region of murine ephrin-B2 (cyto WT; residues 254–336) by pull-down from rat kidney lysate (see Methods). Analysis of the eluted proteins by liquid chromatography with tandem mass spectrometry (LC-MS/MS) led to the identification of several components of the endocytosis machinery including proteins of the AP2 clathrin adaptor complex, clathrin heavy polypeptide, the large GTPase Dynamin 2, the motor protein Myosin VI, and Disabled-2 (Dab2), a clathrin-associated sorting protein[17] (Fig. 3a, b; Supplementary Fig. 3a, b). The interaction with Dab2, which was chosen for further analysis because of its cargo-selective role in endocytosis, required the PDZ binding motif in ephrin-B2, which is essential for many of its functions[24], and was abolished by the exchange of a single amino acid residue at the C-terminus (cyto VS; replacement of valine 336 by serine; Fig. 3c). Since Dab2 does not contain a PDZ domain, we reasoned that its interaction with ephrin-B2 involves another protein acting as molecular scaffold. As it was previously reported that the PAR polarity complex regulates endocytosis[25,26] and can interact with the B-class ligand ephrin-B1[27], which has high homology with ephrin-B2, we examined the role of PAR-3. When lung lysate was incubated with recombinant proteins corresponding to different domains of PAR-3 (Fig. 3d), ephrin-B2, VEGFR2, and VEGFR3 were precipitated with the PDZ domain-containing PAR-3-2N fragment. Ephrin-B2 and VEGFR2 interacted with first PDZ domain and VEGFR3 mainly interacted with third PDZ domain, respectively. In contrast, Dab2 bound to PAR-3-3N, a fragment that contains the aPKC-binding region (Fig. 3a, d). The recognition of molecular cargo is mediated by the PTB domain of Dab2[28]. Accordingly, VEGFR2 and VEGFR3 were precipitated with the recombinant Dab2 PTB domain from cultured mouse ECs stimulated with VEGF-A or VEGF-C (Fig. 3e). In lung lysate, endogenous VEGFR3 was also found associated with Dab2 and PAR-3 by immunoprecipitation, while the interaction of VEGFR3 with Dab2 was strongly diminished in EC-specific inducible PAR-3 loss-of-function mice (*Pard3*$^{i\Delta EC}$) (Fig. 3f). The stimulation with recombinant VEGF-C, which resembles the fully processed form of this ligand that can activate both VEGFR2 and VEGFR3[29], increased the association of immunoprecipitated VEGFR2 with VEGFR3 and the clathrin heavy chain, which was strongly diminished after siRNA-mediated knockdown of Dab2 expression (Fig. 3g).

Angiogenesis and VEGF receptor internalisation require Dab2 and PAR-3

Next, we examined the roles of Dab2 and PAR-3 in VEGF receptor internalisation. While Alexa dye-coupled VEGF-A and VEGF-C were readily taken up by cultured mouse control ECs, knockdown (KD) of *Pard3* or *Dab2* significantly decreased the perinuclear accumulation of VEGF-A and VEGF-C (Fig. 4a–c). Surface biotinylation experiments further confirmed that VEGF-C-induced internalisation of VEGFR3 and VEGFR2 was impaired in *Dab2* KD or *Pard3* KD cells (Fig. 4d, e). In line with previous reports showing that VEGF receptor internalisation is required for the full activation of certain downstream signals[12,13,30], VEGF-A or VEGF-C-induced activation of the small GTPase Rac1 was markedly reduced in *Dab2* KD or *Pard3* KD ECs (Fig. 4f). Likewise, VEGF-A or VEGF-C-induced activation of mitogen-activated protein kinase ERK1/2, a signal linked to EC proliferation[31], was reduced in *Dab2* or *Pard3* KD cells, while no significant effect on AKT phosphorylation was observed (Supplementary Fig. 4a–c). VEGF stimulation also induced the phosphorylation of aPKC in control but not in *Dab2* KD cells (Supplementary Fig. 4b). Further arguing for a link between VEGFR2 signalling and aPKC activation, phospho-aPKC staining was reduced in P6 *Flk1*$^{i\Delta EC}$ retinal vessels (Supplementary Fig. 4d).

Because gene targeting of Dab2 or PAR-3 in the embryonic endothelium caused severe vascular defects (Supplementary Fig. 5a, b and data not shown), we used inducible EC-specific genetic models to characterize the function of the genes in the postnatal retinal vasculature, which is one of the most established system for the analysis of sprouting angiogenesis[16]. Whole mount staining confirmed the expression of Dab2 or PAR-3 in the P6 control retinal vasculature without appreciable differences between central and peripheral vessels (Fig. 5a, b and Supplementary Fig. 5c). Specific endothelial antibody signals were absent in *Dab2* KO mice (*Dab2*$^{i\Delta EC}$) or *Pard3* KO mice (*Pard3*$^{i\Delta EC}$), respectively (Fig. 5a, b). Despite the limited time period between tamoxifen injection at P1–P3 and phenotypic analysis at P6, the *Dab2*$^{i\Delta EC}$ or *Pard3*$^{i\Delta EC}$ retinal vasculature showed pronounced reductions in the size and complexity of the endothelial network, tip cell number, sprout length, number of filopodia and endothelial proliferation (Fig. 5a–d and Supplementary Fig. 5d, e), which resembled defects previously reported for *Efnb2* mutant mice[12,13]. Linking these defects to altered VEGF receptor endocytosis, the uptake of intraocularly injected, Alexa dye-labelled VEGF-A or VEGF-C was significantly reduced in endothelial cells at the P6 *Dab2*$^{i\Delta EC}$ or *Pard3*$^{i\Delta EC}$ angiogenic front (Fig. 5e, f and Supplementary Fig. 5f). Moreover, VEGFR2 and VEGFR3 immunostaining was enhanced in mutant sprouts (Supplementary Fig. 6a–c). These changes probably do not reflect altered expression of the *Flk1/Vegfr2* or *Flt4/Vegfr3* genes, because transcript levels were not significantly altered in *Dab2*$^{i\Delta EC}$ or *Pard3*$^{i\Delta EC}$ mutant lung lysates (data not shown).

Negative regulation of VEGF receptor endocytosis by atypical PKC

The identification of Dab2 and PAR-3 as regulators of VEGF receptor endocytosis raised the question whether their activity was constitutively induced by ligand binding or actively regulated. Indicating a role of the latter, atypical protein kinase C, namely PKCλ or PKCζ, effectively phosphorylated the Dab2 PTB protein fragment *in vitro*, which strongly reduced its interaction with VEGFR2 or VEGFR3 (Fig. 6a and data not shown). Western blot analysis revealed Serine 24 at the border of the Dab2 PTB domain as one of the phosphorylation sites (Fig. 6a), and, accordingly, blocking of endogenous aPKC in cultured mouse ECs strongly reduced Ser24 phosphorylation of Dab2 (Fig. 6b). For functional studies, we generated inducible EC-specific PKCλ loss-of function-mice (*Prkci*$^{i\Delta EC}$), in which gene inactivation was triggered at P1-3. The amount of Dab2 co-immunoprecipitated with VEGFR3 from P6 *Prkci*$^{i\Delta EC}$ lung lysate was strongly increased compared to control littermate samples (Fig. 6c). Arguing further for a negative regulation of the Dab2-cargo interaction by aPKC, VEGFR3-associated Dab2 lacked detectable Ser24 phosphorylation (Fig. 6c). Surface biotinylation assays showed that inhibition of aPKC activity in cultured ECs led to a significant acceleration of ligand-induced VEGFR2 and VEGFR3 internalisation (Fig. 6d). This was accompanied by increased VEGF-A or VEGF-C-induced activation of mitogen-activated protein kinase ERK1/2 (Fig. 6e), a signal linked to EC proliferation[31]. VEGF-A-induced proliferation was reduced in cultured *Dab2* and *Pard3* KD mouse ECs (data not shown).

To gain insight into the spatial pattern of aPKC activity *in vivo*, we immunostained retinas with phospho-aPKC antibody. Supporting the validity of this approach, signals corresponding to total aPKC (PKCλ and PKCζ) and activated aPKC (autophosphorylated at Thr560 or Thr403 in PKCλ) were strongly reduced in the retinal vasculature of EC-specific *Prkci*$^{i\Delta EC}$ mutants (Fig. 6f and data not shown). Phospho-aPKC immunofluorescence showed striking regional differences in the retinal vasculature. While total aPKC staining decorated ECs both at the angiogenic front and in peripheral sprouts (Fig. 6g), phospho-Thr560 and phospho-Thr403 signals were very low in ECs at the angiogenic front in comparison to the more established vessels of the central retina (Fig. 6h and Supplementary Fig. 6d). These findings suggested that higher aPKC activity in ECs of the central retina

might reduce ligand-induced VEGF receptor internalisation preferentially in this area. Indeed, the accumulation of Alexa dye-labelled VEGF-A or VEGF-C was significantly increased in the endothelium of the *Prkci*$^{i\Delta EC}$ central plexus relative to control littermates (Fig. 7a–c). In contrast, the uptake of labelled VEGFs was not significantly altered at the *Prkci*$^{i\Delta EC}$ angiogenic front (Fig. 7c). The further investigate the role of aPKC as a negative regulator of VEGF receptor internalisation, the uptake of Alexa-labelled VEGF-A in cultured ECs was examined in a pulse-chase experiment involving 3 min of stimulation (pulse) followed by 15 min incubation in serum-free growth medium (chase). aPKC inhibitor-treated cells, but not vehicle-treated control ECs, showed substantial VEGF-A uptake under these conditions (Supplementary Fig. 7a, b).

Loss of PKCλ in the postnatal endothelium also led to changes in the immunostaining levels of VEGF receptors. VEGFR2 and VEGFR3 signals were significantly reduced in vessels of the central retina but not at the angiogenic front (Supplementary Fig. 7c, d). Moreover, 2 hours after inhibition of protein degradation by intraocular injection of MG132, VEGFR2 levels in mutant central vessels were partially restored. Changes for VEGFR3 in the central retina of MG132-treated *Prkci*$^{i\Delta EC}$ mice, however, were not significant under the same conditions (Supplementary Fig. 7c, d).

Next, we investigated the morphological changes in the *Prkci*$^{i\Delta EC}$ retinal vasculature. The size and complexity of the endothelial network were reduced predominantly in the centre at P6, whereas tip cell number, sprout length and number of filopodia at the angiogenic front were not significantly altered (Fig. 7d–g). Vessels in the central retina, the region of enhanced VEGF internalisation, showed numerous ectopic sprouts, filopodia-extending tip cells and empty collagen IV matrix sleeves (Fig. 7d–g and Supplementary Fig. 8a, b). The latter is a mark for retracted sprouts as well as collapsed, unstable vessels, which may explain the hypovascularity of the *Prkci*$^{i\Delta EC}$ central retinal vessel network despite enhanced sprouting. This defect is reminiscent of ephrin-B2 gain-of-function mice, in which the transgenic overexpression of the ligand in ECs led to enhanced but unstable sprouting, the appearance of numerous empty collagen IV sleeves and hypovascularity[13]. Ectopic sprouting in the central retina of *Prkci*$^{i\Delta EC}$ mutants was suppressed by the simultaneous targeting of the *Pard3* or *Dab2* genes, respectively (Fig. 8a). Furthermore, anti-VE-cadherin immunostaining of P6 *Prkci*$^{i\Delta EC}$ and *Pard3*$^{i\Delta EC}$ retinas did not reveal appreciable differences between mutants and the corresponding control littermates (Supplementary Fig. 8c, d). Thus, while PAR-3 and PKCλ are likely to play numerous distinct roles in the vasculature, the disruption of endothelial cell-cell contacts is not an overt explanation for ectopic sprouting and filopodia formation in *Prkci*$^{i\Delta EC}$ mutants.

Discussion

In angiogenesis as well as many other morphogenetic processes, individual cells or groups from an initially homogeneous population acquire distinct behaviours but act collectively, which enables complex and highly coordinated biological tasks[4,32]. At the edge (front) of the growing retinal vasculature, leading, filopodia-extending tip cells and endothelial proliferation promote the extension of the vessel network. Conversely, vessels in the central retina (and elsewhere at the end of development) acquire a quiescent and mature phenotype. Our results indicate that the differential regulation of surface receptor endocytosis might help to assign certain cells to specific functional roles. High rates of receptor turnover and signalling might be key features of cells that lead migrating cell clusters and therefore need to respond strongly and quickly to signals in their tissue environment. Such dynamic responses also require the rapid clearing of activated receptors, which might otherwise prevent necessary adjustments in the speed or direction of migration. Our data also suggests that the distinct behaviours of actively growing and maturing vessels are not exclusively

controlled by the proximity of ECs to tissue-derived angiogenic growth factors such as VEGFs, which are known to play important roles in vessel patterning. Instead, we propose here that the differential regulation of VEGF receptor endocytosis through ephrin-B2, Dab2, PAR-3 and aPKC helps to assign specific tasks to endothelial cells (Fig. 8b).

Given the important role of aPKC activity in VEGF receptor endocytosis and signalling, it will be important to determine the relevant regulators that act further upstream. Of the numerous direct and indirect molecular interactions known, the association of the PAR-3/PAR-6/aPKC polarity complex with junctional proteins and, in particular, cadherin family cell adhesion molecules are noteworthy[33,34]. Junctions in more established vessels have presumably higher stability and might sustain or recruit more complexes containing active aPKC. Indeed, phosphorylated aPKC was strongly reduced in cultured VE-cadherin-deficient ECs[35]. In support of this observation, endothelial phospho-aPKC immunostaining was strongly reduced in the central retina of EC-specific, inducible *Cdh5* (VE-cadherin) mutant mice (Fig. 8c). However, it has been also reported that the VE-cadherin-associated polarity complex lacks aPKC in cultured ECs[36], which could indicate an indirect connection between the cadherin and aPKC activation. VEGF signalling emerges as another upstream regulator of aPKC. VEGF-A stimulation increases phospho-aPKC levels[37], but with a slower kinetics compared to AKT or ERK phosphorylation (Supplementary Fig. 4b), and phospho-aPKC immunosignals were reduced in *Flk1*$^{i\Delta EC}$ vessels (Supplementary Fig. 4d). Thus, it is well possible that VEGF receptor endocytosis and signalling involves a negative feedback loop, in which aPKC dynamically downregulates Dab2-dependent VEGFR2 and VEGFR3 internalisation after a period of signalling. These two examples suggest that multiple upstream stimuli can control the activity of aPKCs and thereby potentially affect the spatial pattern of VEGF receptor endocytosis. It also needs to be considered that Dab2 and PAR complex proteins have numerous known cellular roles besides the regulation of VEGF receptors. Such functions might contribute to the mutant phenotypes reported here.

Alterations in the expression or activity of endocytosis regulators might be relevant in pathological conditions. The vasculature of tumours is often irregularly organised, tortuous and leaky[15,38], which has been linked to enhanced VEGF/VEGFR2 signalling. The PAR complex is also an important signalling hub in cancer that has been proposed to have tumour suppressor function. Accordingly, the loss of polarity genes is associated with hyperproliferation in Drosophila[39]. It should be worthwhile to address whether links between aPKC, the endocytic machinery and growth factor signalling might explain some of the altered properties of tumour cells and vessels. Moreover, Eph/ephrin family molecules, CLASPs and polarity proteins are expressed in a large variety of different cell types and tissues[40–42] and are likely to control a range of different biological processes. For example, it has been recently proposed that Dab2 controls bone morphogenetic protein signalling in the axial vein of early zebrafish embryos[43]. Thus, our findings might well be applicable to other organ systems, morphogenetic processes and receptor pathways.

Methods

Intraocular injections

VEGF-A (ReliaTech, cat. no. 300-076) VEGF-A121 (ReliaTech, cat. No.300-072), and VEGF-C (PeproTech, cat. no. 100-20C) were labelled with the Alexa Fluor 546 Protein Labeling Kit (Invitrogen) according to the manufacturer's instructions. 600 nl of labelled VEGF-A (0.2 mg/ml) together with 100 μM of MG132 (Sigma), labelled VEGF-C (0.2 mg/ml), 100μM of MG132, 100 μM of MG115 (Calbiochem), 300 μM of MiTMAB (Calbiochem), 200 μM of Dynasore (Calbiochem) or 1 mM of Chloroquine (Invivogen) in PBS were injected into the vitreous humour using glass capillary pipettes with a micromanipulator (Drummond Scientific Co.). For co-injection of proteasome inhibitors

with 50 μg/ml of cycloheximide (Calbiochem), cyclohexamide was injected 1 hour before the proteasome inhibitors.

Quantitative PCR analysis

For the analysis of mRNA relative expression levels, total RNA from control and mutant retinas was isolated with the RNeasy Mini Kit (QIAGEN), and 500 ng per reaction was used to generate cDNA with the SuperScript III First-Strand Synthesis System (Invitrogen) and oligo(dT) primers. Quantitative PCR with reverse transcription (qRT–PCR) was performed by using an ABI PRISM 7900HT Sequence Detection System. TaqMan gene expression assays for murine *Gapdh*, *Vegfr3*, *Flt4 and Vegfa* were used in combination with TaqMan Gene Expression Master Mix (Applied Biosystems). Gene expression was normalized to the endogenous *Gapdh*. Relative expression differences represent the average of results obtained for at least three independent animals per group. For each animal/cDNA, two separate qRT–PCR plates were used, with duplicate reactions for each gene.

Affinity purification

Adult rat kidney cytosol, which was concentrated by ammonium sulfate precipitation, was loaded onto a Glutathione Sepharose (GE healthcare) affinity column on which 6 nmol of GST, GST-ephrin-B2 cyto wt, or -ephrin-B2 cyto VS were immobilised. After washing the column three times with wash buffer (20 mM Tris-HCl [pH 7.4], 1 mM EDTA, 1 mM dithiothreitol) and three times with wash buffer containing 50 mM NaCl, bound proteins were eluted three times with wash buffer containing 500 mM NaCl. The first eluates were subjected to SDS-PAGE, and the isolated proteins were detected by silver staining, Western blot with anti-Dab2 antibodies (SantaCruz, H-110) or LC-MS/MS analysis.

Mouse genetics

Cdh5(PAC)-CreERT2[13] or *Pdgfb-iCre*[44] transgenics, as indicated in the Figure legends, were bred into a background of animals carrying loxP-flanked *Flk1*[45], *Cdh5* (generated by D.Vestweber and currently unpublished), *Dab2*[46], *Pard3*[47] and *Prkci* alleles[48]. Images shown in the figures represent data obtained with *Pdgfb-iCre* transgenes unless indicated otherwise. Cre activity in newborn mice was induced by three consecutive intraperitoneal tamoxifen (1mg/ml in ethanol/peanut oil) injections of 50 μl given on P1, P2 and P3. The phenotypes of mutant mice were analysed at postnatal stages P6, as indicated. There are no known sex-specific differences in retinal angiogenesis, which allowed us to combine male and female mice for analysis. Tamoxifen-injected Cre- littermate animals were used as control.

All animal experiments were performed in compliance with the relevant laws and institutional guidelines and were approved by local animal ethics committees.

HPLC and mass spectrometry

Peptides from affinity-purified proteins were prepared according to the Filter Aided Sample Preparation method (FASP)[49] in combination with an additional anion exchange fractionation step[50]. Reverse-phase nano-LC-MS/MS analysis of peptides was performed using an EasyLC nanoflow LC system (Proxeon), which was coupled to a LTQ Orbitrap Velos mass spectrometer (Thermo Fisher Scientific) equipped with a nanoelectrospray source (Proxeon). Chromatographic separation of peptides was achieved on in house packed fused silica capillary columns (length 15cm; ID 75μm) filled with reverse-phase ReproSil-Pur C18-AQ 3 μm resin (Dr. Maisch GmbH). Peptide mixtures were loaded at a maximum backpressure of 200 bar and then eluted with a linear gradient at a flow rate of 0.25μl/min. The mass spectrometer was operated in the data-dependent mode to automatically measure

MS and MS2. LTQ-FT full scan MS spectra (from m/z 350 to m/z 1650) were acquired with a resolution of R = 60,000 at m/z 400. The 15 most intense ions were isolated and fragmented in the linear ion trap by using collision-induced dissociation. Raw data files were converted to Mascot generic format files with MaxQuant v1.0.13.13[51] and the Mascot search engine (version 2.2.02) was used for database searches and protein identification (IPI 3.60 mouse). The search parameters were: Trypsin as cleavage reagent, a maximum of 2 missed cleavages and a minimum of 6 amino acids per peptide, carbamidomethylation of cysteine residues were set as fixed modification and oxidation of methionines was selected as variable modification. The maximum allowed mass deviation was 10ppm for MS and 0.5 Da for MS/MS scans.

Immunoprecipitation

For immunoprecipitation of VEGFR2 and VEGFR3, 5–10 μg of antibodies (VEGFR2: R&D, AF644 and MAB4431; VEGFR3: R&D, AF743) were cross-linked to protein A/G sepharose beads by using Protein A/G HP SpinTrap Buffer kit (GE healthcare) according to the manufacturer's instructions. For the co-immunoprecipitation of VEGFR2, VEGFR3 and the clathrin heavy chain (CHC), *Efnb2* lox/lox cells[13] (1×10^6 cells/10-cm dish) were seeded and incubated for 24 hours. Before stimulation, cells were deprived of serum for 24 hrs. Cells were then incubated in serum-free growth medium containing 100ng/ml of VEGF-C (Peprotech) at 37 °C for 5 min, washed with ice-cold PBS and lysed with 800 μl of lysis buffer (50 mM Tris-HCl [pH 7.4], 1% NP-40, 150 mM NaCl, protease inhibitor cocktail (Sigma, P2714, 1:100), phosphatase inhibitor cocktail (Calbiochem, 524629, 1:50). The lysates were centrifuged at 20,000 × g for 10 min at 4 °C, and supernatants were incubated with protein G sepharose beads crosslinked to VEGFR3 antibody at 4 °C for 1 hr. The beads were washed three times with an excess of lysis buffer and eluted with 60 μl of SDS sample solution. 20 μl of each eluate was subjected to SDS-PAGE, followed by immunoblotting with antibodies recognizing VEGFR3 (eBioscience, ALF4), VEGFR2 (Cell Signaling, 55B11) and CHC (Becton Dickinson, 610500) antibody.

For immunoprecipitation of PAR-3, VEGFR3 and Dab2, P6 mouse lung lysates were generated with lysis buffer (50 mM Tris-HCl [pH 7.4], 0.1% SDS, 1% NP-40, 150 mM NaCl, protease inhibitor cocktail (Sigma, P2714, 1:100), phosphatase inhibitor cocktail (Calbiochem, 524629, 1:50) and cleared by centrifugation at 100,00 × g for 30 min at 4 °C. The soluble supernatants were incubated protein A/G sepharose beads crosslinked to antibodies for 1 hr at 4 °C, washed 3 times with wash buffer (50 mM Tris-HCl [pH 7.4], 1% NP-40, 150 mM NaCl, protease inhibitor cocktail (Sigma, P2714, 1:100), phosphatase inhibitor cocktail (Calbiochem, 524629, 1:50), and eluted by boiling in sample buffer for SDS page. Immunoblot analysis with the indicated antibodes was performed.

siRNA transfection and characterisation of signalling

Oligonucleotide siRNA duplexes were purchased from Invitrogen. siRNA sequences were as follows: siPAR-3#1, 5′-GACCCAGCUUUAACUGGCCUUUCCA-3′; siPAR-3#2, 5'-CGACAGCUGGCUUUCUCAAGCAGAA-3'; siDab2#1, 5′-GCUGAACCAUUAGUCGUCGAUCUUA-3′; siDab2#2, 5'-CGGCCUAAACCUAAAGCAU-3'. The transfection of siRNA in *Efnb2* lox/lox cells was carried out with Oligofectamine reagent (Invitrogen), according to the manufacturer's instructions. Cells were analysed at 2 days after transfection.

For signalling studies in cultured cells, control ($Efnb2^{lox/lox}$) cells were seeded at a density of 3.0×10^5 in 6-cm dishes and incubated for 24 hrs. Before stimulation, cells were deprived of serum for a further 24 hrs. For the aPKC inhibitor treatment, serum-deprived cells were treated with 5 μM of aPKC inhibitor (Merk, 539624) for 30 min. Cells were then incubated

in serum-free growth medium containing 100 ng/ml of VEGF-A or VEGF-C at 37 °C for the indicated times, collected with 100 μl of 1 × SDS sample buffer and subjected to immunoblotting with phospho-AKT (Ser 473) antibody (Cell Signaling, 4060, 1:2000), phospho-p44/42 MAPK antibody (Cell Signaling, 4370, 1:1000), AKT antibody (Cell Signaling, 9272, 1:1000), p44/42 MAPK antibody (Cell Signaling, 4695, 1:1000), phosho-aPKC antibody (Cell Signaling, 9378, 1:1000), and total aPKC antibody (Becton Dickinson, 610207, 1:1000).

VEGF-A uptake in cultured cells

For Alexa-labelled VEGF-A uptake in cultured cells, control (*Efnb2*$^{lox/lox}$) cells were seeded on cover slips at a density of 3.0×10^5 in 6-cm dishes and incubated for 24 hrs. After siRNA transfection, cells were deprived of serum for 24 hrs before they were incubated in serum-free growth medium containing 4 μg/ml of Alexa-labelled VEGF-A or VEGF-C at 37 °C for 30 min. For the pulse-chase analysis, serum-deprived cells were treated with 5 μM of aPKC inhibitor (Merk, 539624) for 30 min and stimulated with 4 μg/ml of Alexa-labelled VEGF-A for 3 min. After washing with serum-free growth medium, cells were further incubated for 15 min. Finally, cells were fixed with 4% PFA for 10 min on ice and stained with Alexa-coupled phallodin (Invitrogen) and DAPI.

Pull down assays

GST pull down assay was performed as previously described[52]. Briefly, GST-fusion proteins were immobilised onto Glutathione Sepharose beads. The beads were incubated with *Efnb2* lox/lox cells[13] or lung lysate. Beads were washed three times with lysis buffer (20 mM Tris-HCl [pH 7.4], 1 mM EDTA, 1 mM dithiothreitol, 150 mM NaCl and 1% NP-40, protease inhibitor cocktail (Sigma, P2714, 1:100) and dissolved into SDS sample buffer. Bound proteins were subjected to Western blot analysis with anti-VEGFR2 (Cell Signaling, 55B11, 1:1000), anti-VEGFR3 (eBioscience, ALF4, 1:1000), anti-Dab2 (SantaCruz, H-110, 1:500), or anti-ephrin-B2 antibodies (Sigma, HPA008999, 1:1000).

For Rac1 pull-downs, *Efnb2* lox/lox cells (1×10^6 cells/10-cm dish) were seeded and incubated for 24 hrs. For stimulation, cells were deprived of serum for 24 hrs, incubated in serum-free growth medium containing 100 ng/ml of VEGF-A or VEGF-C (Peprotech) at 37°C for 5 min, washed with ice-cold PBS, and lysed with 800 μl of lysis buffer (50 mM Tris-HCl [pH 7.4], 20 mM $MgCl_2$, 1% NP-40, 500 mM NaCl, 40 μg/ml purified GST-CRIB, protease inhibitor cocktail (Sigma, P2714, 1:100). Lysates were centrifuged at 20,000 × g for 2 min at 4°C, and supernatants were incubated with Glutathione Sepharose beads at 4°C for 30 min. Beads were washed three times with an excess of wash buffer (50 mM Tris-HCl [pH 7.4], 20 mM $MgCl_2$, 1% NP-40, 500 mM NaCl, protease inhibitor cocktail (Sigma, P2714, 1:100)) and eluted with 45 μl of SDS sample solution. Finally, 20 μl of each eluate was subjected to SDS-PAGE, followed by immunoblotting with anti-Rac1 antibody (Millipore, 05-389, 1:400).

Phosphorylation assay

The reaction was carried out in a 50 μl assay mixture containing 20 mM Tris-HCl (pH 7.4), 5 mM $MgCl_2$, 1 mM EGTA, 1 mM DTT, 0.2 μM recombinant aPKCλ (Millipore), 10 μM ATP, and 1μM purified GST-Dab2 PTB domain for 60 min at 30°C. The reaction was stopped by the addition of SDS sample buffer and the products were subjected to SDS-PAGE, followed by a silver staining. Radiolabelled bands were visualised by an image analyser (GE healthcare). Alternatively, assay mixtures were incubated with Glutathione-Sepharose beads and then mixed with cell lysates as described above for 1 hr at 4°C. Bound proteins were eluted with SDS sample buffer and were analysed by immunoblot anti-

VEGFR2 (Cell Signaling, 55B11, 1:1000), anti-VEGFR3 (eBioscience, ALF4, 1:1000) or anti-phosho-Ser24 Dab2 antibodies (SantaCruz, sc-32573, 1:1000).

Staining of tissues and cells

For retina staining, eyes were dissected and fixed in 4% PFA for 2 hrs at room temperature or on ice as described previously[53]. For VEGFR2 staining, retinas were fixed with 4% PFA on ice for 20 min. Briefly, retinas were dissected, permeabilised and blocked in 1% BSA (Sigma, A4378) and 0.3% Triton X-100 overnight at 4 °C with gentle rocking. Next, retinas were washed three times in Pblec buffer (1 mM $CaCl_2$, 1 mM $MgCl_2$, 1 mM $MnCl_2$ and 1% Triton X-100 in PBS) and incubated with biotinylated isolectin B4 (Vector, B-1205, *Griffonia simlicifolia* lectin I, 1:25), overnight at 4°C with gentle rocking. Retinas were washed five times with 0.5% BSA and 0.15% Triton X-100 and incubated with Alexa-Fluor-coupled streptavidin (Invitrogen, 1:100) in blocking buffer for 2 hrs at room temperature. Primary antibodies diluted in blocking buffer were applied overnight at 4°C: rabbit anti-VEGFR2 (Cell Signaling, 55B11, 1:100), rabbit anti-Dab2 (SantaCruz, H-110, 1:100), rabbit anti-PAR-3[52], goat anti-VEGFR3 (R&D Systems, AF 743, 1:50), rabbit anti-collagen IV (Chemicon, AB756P, 1:200), rat VE-cadherin antibody (eBioscience, 555289, 1:100), and rabbit active aPKC (Abcam, ab59412, 1:100; Cell Signaling, 9378, lots 6 and 8, 1:100). After a washing step, retinas were incubated with the corresponding Alexa-Fluor-coupled secondary antibody (Invitrogen, 1:500) in blocking buffer for 2 hrs at room temperature. Nuclei were stained with TO-PRO-3 (Invitrogen, T3605). Retinas were flat-mounted using Fluromount-G (SouthernBiotech, 0100-01).

For the labelling of proliferating cells, P6 pups received intraperitoneal injections with 5-bromo-2′deoxyuridine (Invitrogen, B23151, 300μg BrdU dissolved in 100μl PBS). After 2.5 hours, pups were killed and eyes were dissected and fixed for 2 hrs at room temperature. After isolectin B4 staining, retinas were refixed in 4% PFA for 30 min at room temperature and incubated in 50% formamide, 1× SSC solution at 65°C for 1 hr. Retinas were then incubated in 2N HCl at 37°C for 30 min and neutralised with 0.1M Tris-HCl [pH 8.0] twice for 10 min each. After washing with PBS, retinas were blocked for 2 hrs at room temperature, and incubated with monoclonal mouse anti-BrdU antibodies (Becton Dickinson, 347580, 1:50) diluted in blocking buffer overnight at 4°C with gentle rocking. Next, staining and mounting steps were performed as described above.

Cell surface biotinylation

Cell surface biotinylation was performed on *Efnb2* lox/lox cells (in 100-mm diameter dishes). Surface receptors were labelled with 0.5 mg/ml sulpho-NHS-biotin (Thermo Scientific) according to the manufacturer's instructions. After quenching of excess biotin with 100mM glycine in PBS, the cells were dissolved in 0.8ml lysis buffer (25mM Tris-HCl [pH 7.5], 150mM NaCl, 5mM EDTA-NaOH [pH 8.5] 0.5 % Triton X100, 0.5 % NP-40, 100mM NaF, 10mM $Na_4P_2O_7$, 1mM Na_3VO_4 and protease inhibitor cocktail (Sigma, P2714, 1:100). The lysates were precipitated with streptavidin agarose beads (Invitrogen), and the precipitates were analysed by immunoblot with anti-ephrin-B2 (R&D, AF496, 1:500), anti-VEGFR3 (eBioscience, ALF4, 1:1000) or anti-VEGFR2 antibodies (Cell Signaling, 55B11, 1:1000).

Quantification, statistical analysis and image processing

Volocity (Improvision), Photoshop CS and Illustrator CS (Adobe) software were used for image processing in compliance with general guidelines for image processing. Data are based on at least three independent experiments or three mutant and control animals for each stage and result shown. The data are presented as mean ± S.D. Statistical differences were evaluated using Student's *t*-test for comparisons of two groups, or analysis of variance

(ANOVA) and appropriate *post hoc* analyses for comparisons of more than two groups. $P<0.05$ was considered significant.

Analysis of branching points, tips, filopodia and EC-covered area were performed with Volocity software (Improvision). Tips were defined as sprouting endothelial cells with filopodial extensions. The sprouts were defined as protrusive endothelial cells above the angiogenic front line. All quantifications were done using high-resolution confocal images and thin z-section of the sample.

Supplementary Material

Refer to Web version on PubMed Central for supplementary material.

Acknowledgments

We thank K. Ebnet and T. Nishioka for reagents and discussions. The Max Planck Society, the German Research Foundation program SFB 629 (RHA), the EMBO LTF program, the Japan Society for the Promotion of Science (MN), and the US National Institutes of Health (JAC) have provided funding.

References

1. Palamidessi A, et al. Endocytic trafficking of Rac is required for the spatial restriction of signaling in cell migration. Cell. 2008; 134:135–147. [PubMed: 18614017]
2. Le Roy C, Wrana JL. Clathrin- and non-clathrin-mediated endocytic regulation of cell signalling. Nat. Rev. Mol. Cell Biol. 2005; 6:112–126. [PubMed: 15687999]
3. Bush JO, Soriano P. Ephrin-B1 forward signaling regulates craniofacial morphogenesis by controlling cell proliferation across Eph-ephrin boundaries. Genes Dev. 2010; 24:2068–2080. [PubMed: 20844017]
4. Bryant DM, Mostov KE. From cells to organs: building polarized tissue. Nat. Rev. Mol. Cell Biol. 2008; 9:887–901. [PubMed: 18946477]
5. Olsson AK, Dimberg A, Kreuger J, Claesson-Welsh L. VEGF receptor signalling - in control of vascular function. Nat. Rev. Mol. Cell Biol. 2006; 7:359–371. [PubMed: 16633338]
6. Lohela M, Bry M, Tammela T, Alitalo K. VEGFs and receptors involved in angiogenesis versus lymphangiogenesis. Curr. Opin. Cell Biol. 2009; 21:154–165. [PubMed: 19230644]
7. Nilsson I, et al. VEGF receptor 2/-3 heterodimers detected in situ by proximity ligation on angiogenic sprouts. EMBO J. 2010; 29:1377–1388. [PubMed: 20224550]
8. Jakobsson L, et al. Endothelial cells dynamically compete for the tip cell position during angiogenic sprouting. Nat Cell Biol. 12:943–953. [PubMed: 20871601]
9. Hellstrom M, et al. Dll4 signalling through Notch1 regulates formation of tip cells during angiogenesis. Nature. 2007; 445:776–780. [PubMed: 17259973]
10. Benedito R, et al. The Notch ligands Dll4 and Jagged1 have opposing effects on angiogenesis. Cell. 2009; 137:1124–1135. [PubMed: 19524514]
11. Jakobsson L, Bentley K, Gerhardt H. VEGFRs and Notch: a dynamic collaboration in vascular patterning. Biochem. Soc. Trans. 2009; 37:1233–1236. [PubMed: 19909253]
12. Sawamiphak S, et al. Ephrin-B2 regulates VEGFR2 function in developmental and tumour angiogenesis. Nature. 2010; 465:487–491. [PubMed: 20445540]
13. Wang Y, et al. Ephrin-B2 controls VEGF-induced angiogenesis and lymphangiogenesis. Nature. 2010; 465:483–486. [PubMed: 20445537]
14. Bochenek ML, Dickinson S, Astin JW, Adams RH, Nobes CD. Ephrin-B2 regulates endothelial cell morphology and motility independently of Eph-receptor binding. J. Cell Sci. 2010; 123:1235–1246. [PubMed: 20233847]
15. Carmeliet P, De Smet F, Loges S, Mazzone M. Branching morphogenesis and antiangiogenesis candidates: tip cells lead the way. Nat. Rev. Clin. Oncol. 2009; 6:315–326. [PubMed: 19483738]

16. Gerhardt H, et al. VEGF guides angiogenic sprouting utilizing endothelial tip cell filopodia. J. Cell Biol. 2003; 161:1163–1177. [PubMed: 12810700]
17. Traub LM. Sorting it out: AP-2 and alternate clathrin adaptors in endocytic cargo selection. J. Cell Biol. 2003; 163:203–208. [PubMed: 14581447]
18. Stone J, et al. Development of retinal vasculature is mediated by hypoxia-induced vascular endothelial growth factor (VEGF) expression by neuroglia. J. Neurosci. 1995; 15:4738–4747. [PubMed: 7623107]
19. Tammela T, et al. Blocking VEGFR-3 suppresses angiogenic sprouting and vascular network formation. Nature. 2008; 454:656–660. [PubMed: 18594512]
20. Benedito R, et al. Notch-dependent VEGFR3 upregulation allows angiogenesis without VEGF-VEGFR2 signalling. Nature. 2012; 484:110–114. [PubMed: 22426001]
21. Bruns AF, et al. Ligand-stimulated VEGFR2 signaling is regulated by co-ordinated trafficking and proteolysis. Traffic. 2010; 11:161–174. [PubMed: 19883397]
22. Manickam V, et al. Regulation of vascular endothelial growth factor receptor 2 trafficking and angiogenesis by Golgi localized t-SNARE syntaxin 6. Blood. 2011; 117:1425–1435. [PubMed: 21063020]
23. Meyer RD, et al. PEST motif serine and tyrosine phosphorylation controls vascular endothelial growth factor receptor 2 stability and downregulation. Mol. Cell. Biol. 2011; 31:2010–2025. [PubMed: 21402774]
24. Makinen T, et al. PDZ interaction site in ephrinB2 is required for the remodeling of lymphatic vasculature. Genes Dev. 2005; 19:397–410. [PubMed: 15687262]
25. Balklava Z, Pant S, Fares H, Grant BD. Genome-wide analysis identifies a general requirement for polarity proteins in endocytic traffic. Nat. Cell Biol. 2007; 9:1066–1073. [PubMed: 17704769]
26. Nishimura T, Kaibuchi K. Numb controls integrin endocytosis for directional cell migration with aPKC and PAR-3. Dev. Cell. 2007; 13:15–28. [PubMed: 17609107]
27. Lee HS, Nishanian TG, Mood K, Bong YS, Daar IO. EphrinB1 controls cell-cell junctions through the Par polarity complex. Nat. Cell Biol. 2008; 10:979–986. [PubMed: 18604196]
28. Mishra SK, et al. Disabled-2 exhibits the properties of a cargo-selective endocytic clathrin adaptor. EMBO J. 2002; 21:4915–4926. [PubMed: 12234931]
29. Joukov V, et al. Proteolytic processing regulates receptor specificity and activity of VEGF-C. EMBO J. 1997; 16:3898–3911. [PubMed: 9233800]
30. Lanahan AA, et al. VEGF receptor 2 endocytic trafficking regulates arterial morphogenesis. Dev. Cell. 2010; 18:713–724. [PubMed: 20434959]
31. Zachary I, Gliki G. Signaling transduction mechanisms mediating biological actions of the vascular endothelial growth factor family. Cardiovasc. Res. 2001; 49:568–581. [PubMed: 11166270]
32. Friedl P, Gilmour D. Collective cell migration in morphogenesis, regeneration and cancer. Nat. Rev. Mol. Cell Biol. 2009; 10:445–457. [PubMed: 19546857]
33. Suzuki A, Ohno S. The PAR-aPKC system: lessons in polarity. J. Cell Sci. 2006; 119:979–987. [PubMed: 16525119]
34. Goldstein B, Macara IG. The PAR proteins: fundamental players in animal cell polarization. Dev. Cell. 2007; 13:609–622. [PubMed: 17981131]
35. Lampugnani MG, et al. CCM1 regulates vascular-lumen organization by inducing endothelial polarity. J. Cell Sci. 123:1073–1080. [PubMed: 20332120]
36. Iden S, et al. A distinct PAR complex associates physically with VE-cadherin in vertebrate endothelial cells. EMBO Rep. 2006; 7:1239–1246. [PubMed: 17057644]
37. Titchenell PM, et al. Novel atypical PKC inhibitors prevent vascular endothelial growth factor-induced blood-retinal barrier dysfunction. Biochem. J. 2012; 446:455–467. [PubMed: 22721706]
38. Jain RK. Molecular regulation of vessel maturation. Nat. Med. 2003; 9:685–693. [PubMed: 12778167]
39. Aranda V, Nolan ME, Muthuswamy SK. Par complex in cancer: a regulator of normal cell polarity joins the dark side. Oncogene. 2008; 27:6878–6887. [PubMed: 19029931]
40. Pasquale EB. Eph-ephrin bidirectional signaling in physiology and disease. Cell. 2008; 133:38–52. [PubMed: 18394988]

41. Martin-Belmonte F, Mostov K. Regulation of cell polarity during epithelial morphogenesis. Curr. Opin. Cell Biol. 2008; 20:227–234. [PubMed: 18282696]

42. Iden S, Collard JG. Crosstalk between small GTPases and polarity proteins in cell polarization. Nat. Rev. Mol. Cell Biol. 2008; 9:846–859. [PubMed: 18946474]

43. Kim JD, et al. Context-dependent proangiogenic function of bone morphogenetic protein signaling is mediated by disabled homolog 2. Dev. Cell. 2012; 23:441–448. [PubMed: 22898784]

References

44. Claxton S, et al. Efficient, inducible Cre-recombinase activation in vascular endothelium. Genesis. 2008; 46:74–80. [PubMed: 18257043]

45. Haigh JJ, et al. Cortical and retinal defects caused by dosage-dependent reductions in VEGF-A paracrine signaling. Dev. Biol. 2003; 262:225–241. [PubMed: 14550787]

46. Morris SM, Tallquist MD, Rock CO, Cooper JA. Dual roles for the Dab2 adaptor protein in embryonic development and kidney transport. EMBO J. 2002; 21:1555–1564. [PubMed: 11927540]

47. Hirose T, et al. PAR3 is essential for cyst-mediated epicardial development by establishing apical cortical domains. Development. 2006; 133:1389–1398. [PubMed: 16510507]

48. Hashimoto N, et al. PKClambda regulates glucose-induced insulin secretion through modulation of gene expression in pancreatic beta cells. J. Clin. Invest. 2005; 115:138–145. [PubMed: 15630453]

49. Wisniewski JR, Zougman A, Nagaraj N, Mann M. Universal sample preparation method for proteome analysis. Nat. Methods. 2009; 6:359–362. [PubMed: 19377485]

50. Wisniewski JR, Zougman A, Mann M. Combination of FASP and StageTip-based fractionation allows in-depth analysis of the hippocampal membrane proteome. J. Proteome Res. 2009; 8:5674–5678. [PubMed: 19848406]

51. Cox J, Mann M. MaxQuant enables high peptide identification rates, individualized p.p.b.-range mass accuracies and proteome-wide protein quantification. Nat. Biotechnol. 2008; 26:1367–1372. [PubMed: 19029910]

52. Nakayama M, et al. Rho-kinase phosphorylates PAR-3 and disrupts PAR complex formation. Dev. Cell. 2008; 14:205–215. [PubMed: 18267089]

53. Pitulescu ME, Schmidt I, Benedito R, Adams RH. Inducible gene targeting in the neonatal vasculature and analysis of retinal angiogenesis in mice. Nat. Protoc. 2010; 5:1518–1534. [PubMed: 20725067]

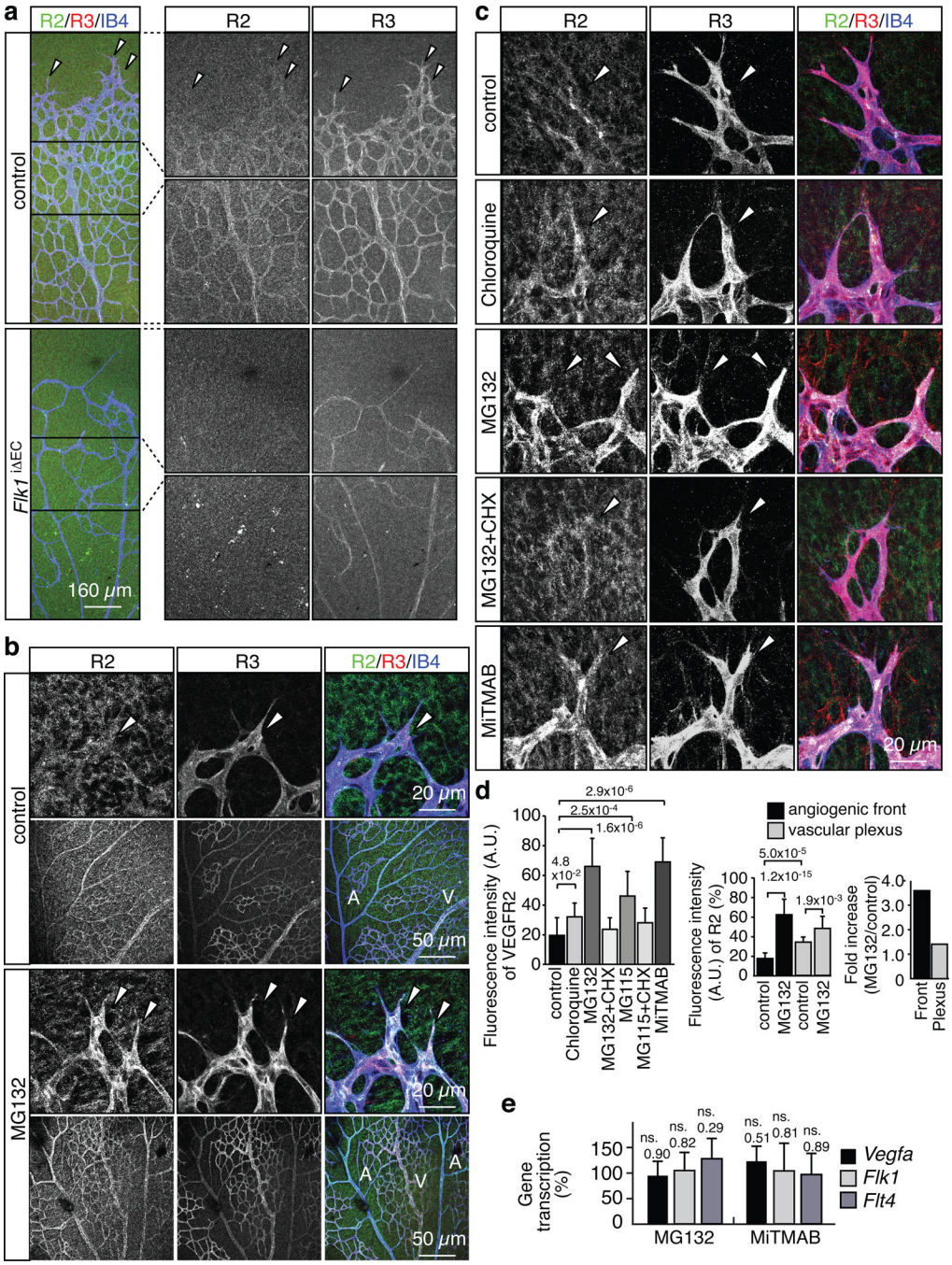

Figure 1. High VEGF receptor turnover in the angiogenic front

a, Anti-VEGFR2 (green), VEGFR3 (red) and IsolectinB4 (IB4; blue) staining of the P6 retinal vasculature. Absent endothelial VEGFR2 immunostaining and strongly decreased VEGFR3 in *Flk1*$^{i\Delta EC}$ retinas. Arrowheads indicate distal sprouts.

b, Strong upregulation of VEGFR2 (green) and VEGFR3 (red) protein levels in P6 vessel sprouts (arrowheads) compared to vessels in central retina at 2 hours after intraocular MG132 injection. ECs, Isolectin B4 (IB4, blue). Arteries (A) and veins (V) are indicated.

c, VEGFR2 and VEGFR3 immunostaining at 2 hours after intraocular injection of the indicated inhibitors. ECs, Isolectin B4 (IB4, blue). Arrowheads mark sprouts.

d, Statistical analysis of VEGFR2 staining as shown in (**b**) and (**c**). Data represent the means ±s.d. of 12 independent experiments. P values, ANOVA.

e, qPCR analysis showing that *Vegfa*, *Vegfr2/Flk1* and *Vegfr3/Flt4* transcript levels in eyes were not significantly increased after MG132 or MiTMAB treatment. Data represent the means±s.d. of 6 independent experiments. P values, two-tailed Student's t-test compared to vehicle-injected controls. ns, not significant.

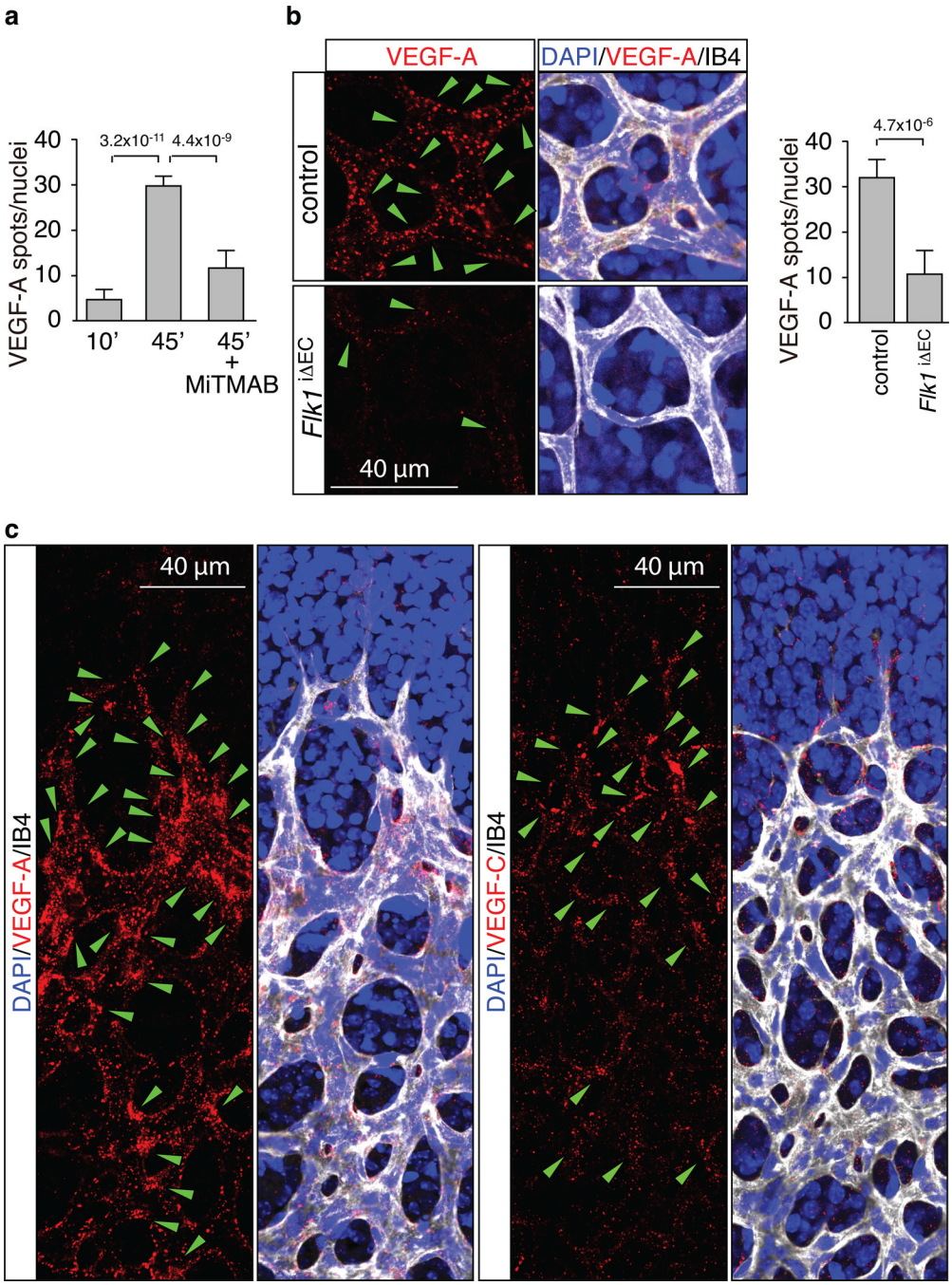

Figure 2. Spatial differences in VEGF uptake in the retina

a, Quantitation of Alexa-labelled VEGF-A in retinal ECs at 10 and 45 min after injection. The formation of intracellular spots was blocked by MiTMAB. Data represent the means ±s.d. of 6 independent experiments. P values, ANOVA.

b, VEGF-A uptake in blood vessels of *Flk*$^{i\Delta EC}$ mice. Green arrowheads indicate internalised Alexa dye-coupled VEGF-A (red). Cell nuclei, DAPI (blue); ECs, Isolectin B4 (IB4, white). Data represent the means±s.d. of 6 independent experiments. P values, two-tailed student t test.

c, Spatial distribution of VEGF-A or VEGF-C (red) uptake in retinal vessels. Green arrowheads indicate internalised label spots. Cell nuclei, DAPI (blue); ECs, Isolectin B4 (IB4, white).

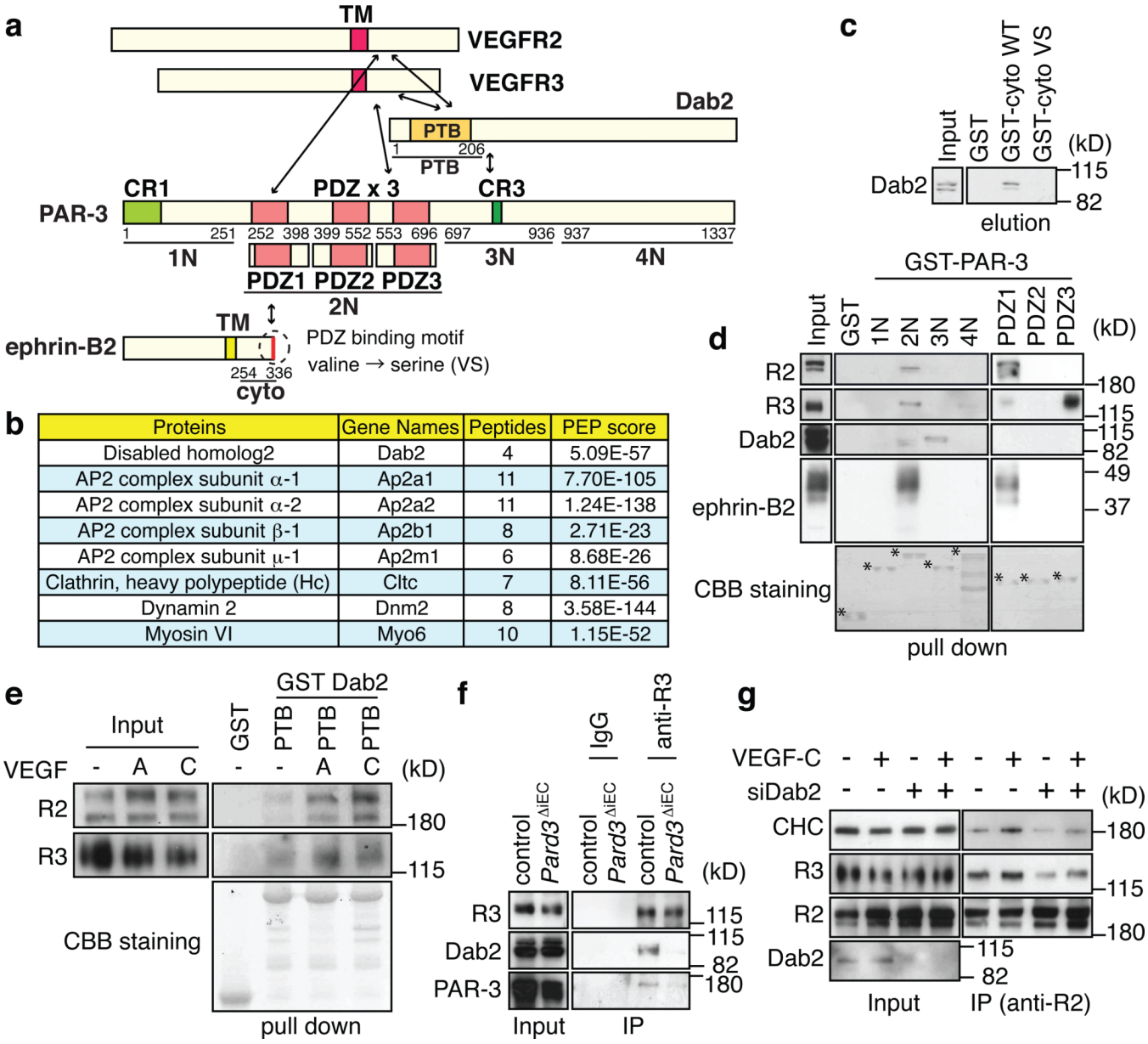

Proteins	Gene Names	Peptides	PEP score
Disabled homolog2	Dab2	4	5.09E-57
AP2 complex subunit α-1	Ap2a1	11	7.70E-105
AP2 complex subunit α-2	Ap2a2	11	1.24E-138
AP2 complex subunit β-1	Ap2b1	8	2.71E-23
AP2 complex subunit μ-1	Ap2m1	6	8.68E-26
Clathrin, heavy polypeptide (Hc)	Cltc	7	8.11E-56
Dynamin 2	Dnm2	8	3.58E-144
Myosin VI	Myo6	10	1.15E-52

Figure 3. Identification of Dab2 and PAR-3 as interactors of ephrin-B2 and VEGF receptors

a, Domain structure and deletion constructs of ephrin-B2, Dab2 and PAR-3. Numbers refer to amino-acid positions in the murine gene products. TM, transmembrane region; CR1, conserved region 1; CR3, conserved region 3; PDZ, PSD-95/Dlg/ZO-1 domains; PTB, phosphotyrosine binding region.

b, Endocytic proteins identified by mass spectrometry. Name of proteins and corresponding genes, the number of peptides identified, and PEP scores are listed.

c, Immunoblotting of affinity-purified samples with anti-Dab2 antibody. Pull-down was performed with GST-cyto WT (GST-fusion protein of cytoplasmic region of ephrin-B2) or GST-cyto VS (mutation in the C-terminal PDZ binding motif of ephrin-B2). Molecular weight marker (kD) is indicated on the right.

d, e, Pull-down analysis with the indicated domains of PAR-3 (**c**) or Dab2 (**d**) fused to GST. Interacting VEGFR2, VEGFR3, Dab2 and ephrin-B2 from cultured mouse ECs were

detected by immunoblot. Binding of VEGF receptors to the GST-PTB domain of Dab2 was enhanced by VEGF. Asterisks mark bait proteins in Coomassie Brilliant Blue (CBB) staining (bottom panels).

f, Immunoprecipitation (IP) of endogenous Dab2 and PAR-3 with VEGFR3 from lung lysate of control mice but not *Pard3*$^{i\Delta EC}$ mutants.

g, Association of PAR-3, clathrin heavy chain (CHC) and VEGFR3 with immunoprecipitated (IP) VEGFR2 in VEGF-C-treated mouse ECs. CHC interaction with VEGFR2 was reduced after knockdown of Dab2 (siDab2).

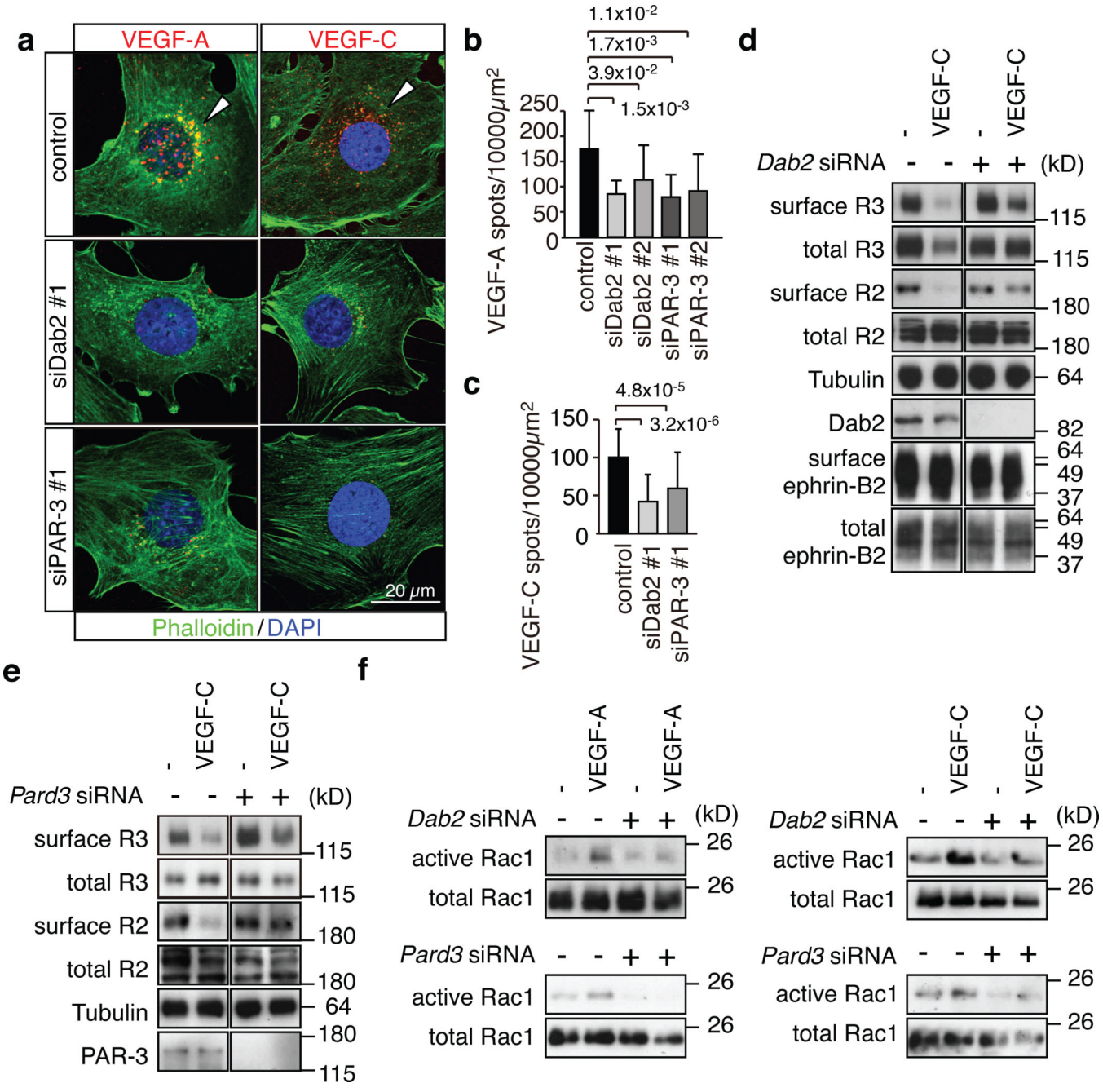

Figure 4. Dab2 and PAR-3 control VEGF receptor internalisation

a, Alexa546-labelled VEGF-A or VEGF-C (red) accumulated in the perinuclear region of control mouse ECs at 30 min after stimulation, which was strongly reduced after knockdown of *Dab2* or *Pard3*. Actin, Phalloidin (green); nuclei, DAPI (blue).

b, c, Quantitation of Alexa546-positive peri-nuclear VEGF-A (**b**) or VEGF-C (**c**) spots. Two different siRNAs were used for *Dab2* and *Pard3* in (**b**). Data represent the means±s.d. of 6 independent experiments. P values, two-tailed Student's t-test. At least 100 cells were scored in each experiment.

d, e, Biochemical detection of biotinylated (surface) VEGFR2 and VEGFR3 in stimulated control and *Dab2* (**d**) or *Pard3* (**e**) KD cells. Antibodies used for immunoblotting and molecular weight marker are indicated.

f, Activation of Rac1 in control and *Dab2* or *Pard3* KD mouse ECs stimulated with VEGF-A or VEGF-C for 5 min, as indicated.

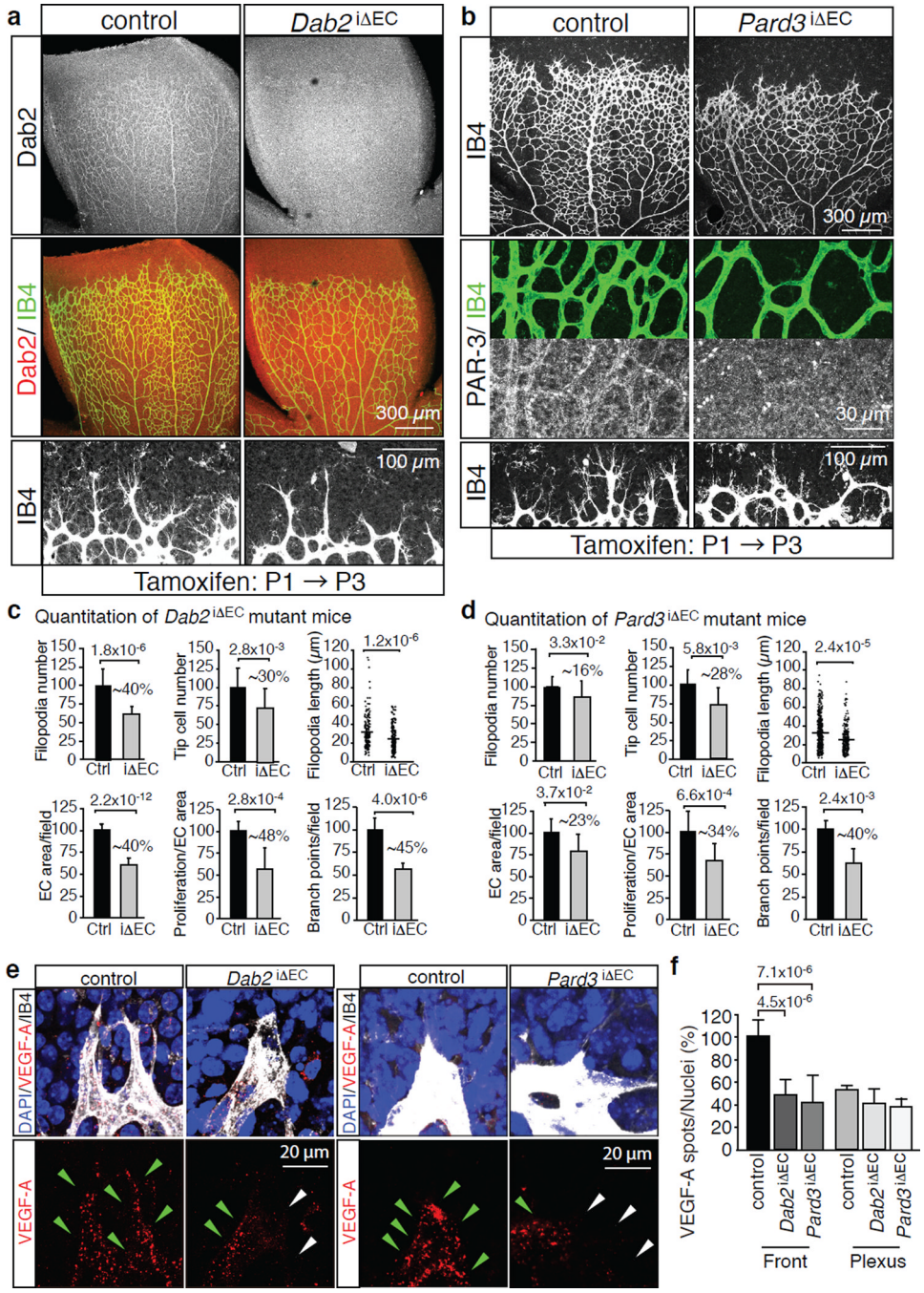

Figure 5. Endothelial Dab2 and PAR-3 regulate angiogenic vessel growth

a, Overview of the P6 control and *Dab2*$^{i\Delta EC}$ retinal vasculature. Anti-Dab2 (white/red) staining is shown in top panels. ECs, Isolectin B4 (IB4). Bottom panels show higher magnification of the angiogenic front.

b, Defects in the P6 *Pard3*$^{i\Delta EC}$ retinal vasculature. Anti-PAR-3 and IB4 (green) staining in middle panels show successful deletion of PAR-3 in *Pard3*$^{i\Delta EC}$ vessels. Residual round signals correspond to autofluorescent blood cells. Bottom panels show higher magnification of the angiogenic front.

c, d, Quantitation of filopodia number and length, tip cell number, EC-covered area, EC proliferation and vessels branch points in *Dab2* mutant (iΔEC) (**c**) or *Pard3* mutant (**d**) retinas compared to the corresponding control littermates (Ctrl). *Dab2* mutant n=7, *Pard3* mutant n=3. Percentage of reduction is indicated. Data represent the means±s.d. P values, two-tailed Student's t-test.

e, Reduced uptake of labelled VEGF-A (red) at the *Dab2*$^{i\Delta EC}$ or *Pard3*$^{i\Delta EC}$ angiogenic front compared to control littermates. Green arrowheads indicate VEGF-A spots, white arrowheads marks ECs with no or little uptake.

f, Statistical analysis of internalised Alexa-coupled VEGF-A in the angiogenic front and central plexus. Data represent the means±s.d. of 6 independent experiments. P values, two-tailed Student's t-test.

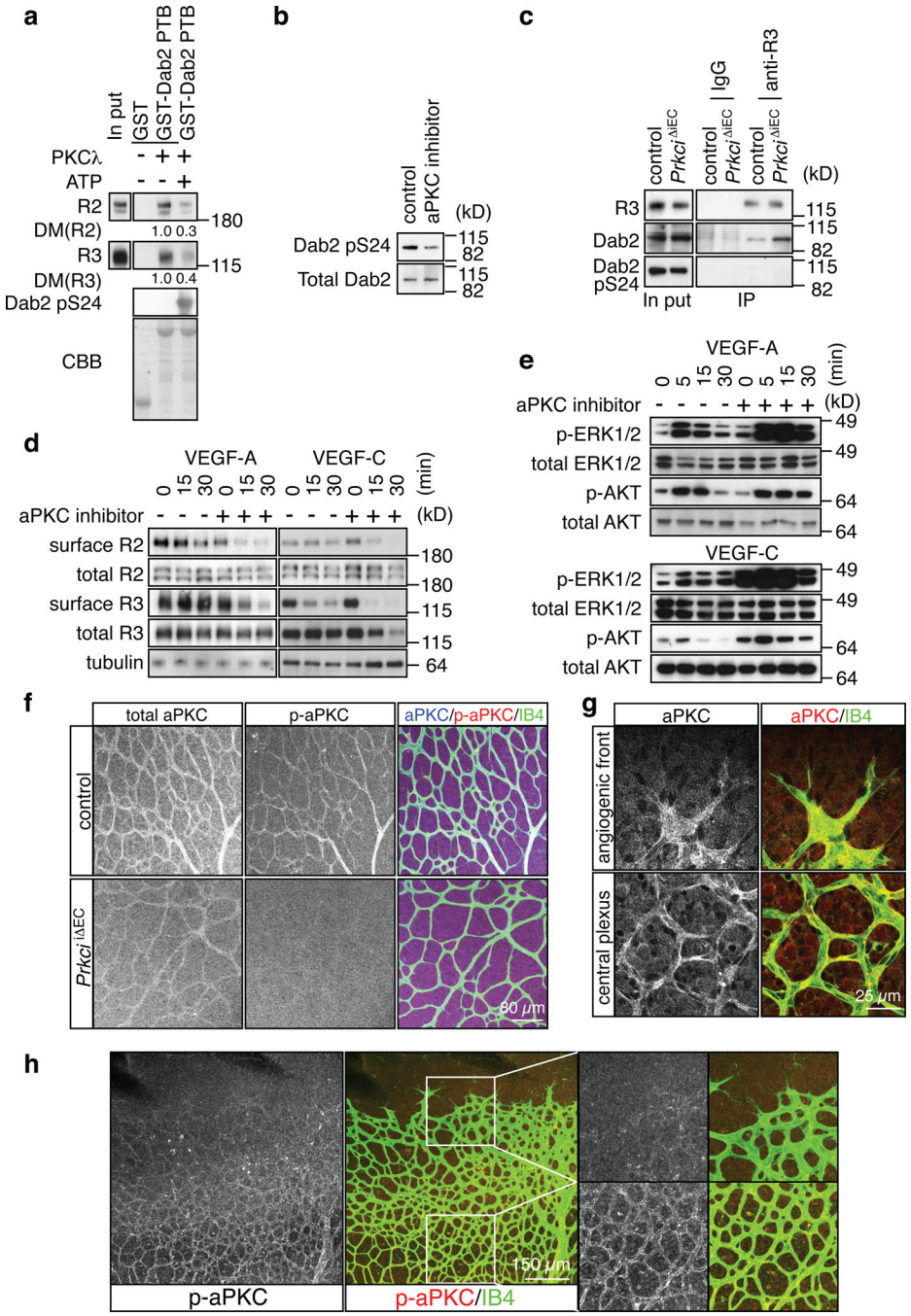

Figure 6. Negative regulation of VEGF receptor internalisation by aPKC

a, Phosphorylation of a GST-Dab2 fusion protein by recombinant PKCλ reduced its interaction with VEGFR3 and VEGFR2 in pull down assays. Densiometric (DM) values are shown below bands. ATP for the kinase activation was added (+) or absent (−), as indicated. CBB, Coomassie Brilliant Blue staining of GST fusion proteins.

b, Western blot showing reduced Dab2 phoshorylation at Serine 24 (pS24) in cultured ECs after 30 min incubation with 5μM aPKC inhibitor.

c, Association of Dab2 with immunoprecipitated VEGFR3 (anti-R3) was enhanced in *Prkci*$^{i\Delta EC}$ lung lysate compared to control littermates. No specific bands were

immunoprecipitated with IgG. VEGFR3-associated Dab2 lacked detectable phosphorylation in Ser24 (pS24).

d, Effect of aPKC inhibition on VEGF-A- or VEGF-C-induced VEGF receptor internalisation at indicated time points. Cells were preincubated with 5 μM of aPKC inhibitor for 30 min. Surface VEGFR2 (R2) and VEGFR3 (R3) were identified by biotinylation.

e, Increased activation of MAP kinase (p-ERK1/2) by VEGF-A or VEGF-C after aPKC inhibition in cultured mouse ECs. Effects on AKT phosphorylation were comparably modest. Total ERK1/2 and AKT are shown as loading controls. Molecular weight marker (kD) is indicated.

f, Anti-aPKC (total), anti-phospho-aPKC (p-aPKC, Thr560) and Isolectin B4 (IB4) staining of the P6 control and *Prkci*$^{i\Delta EC}$ retinal vasculature.

g, Anti-aPKC immunostaining (red) labels ECs (IB4, green) at the angiogenic front and in the central retinal plexus.

h, Phospho-aPKC (p-aPKC, Thr560) immunosignals were weak at the angiogenic front in comparison to vessels of the central plexus. Higher magnification of p-aPKC signals and merged channels in insets is shown on the right.

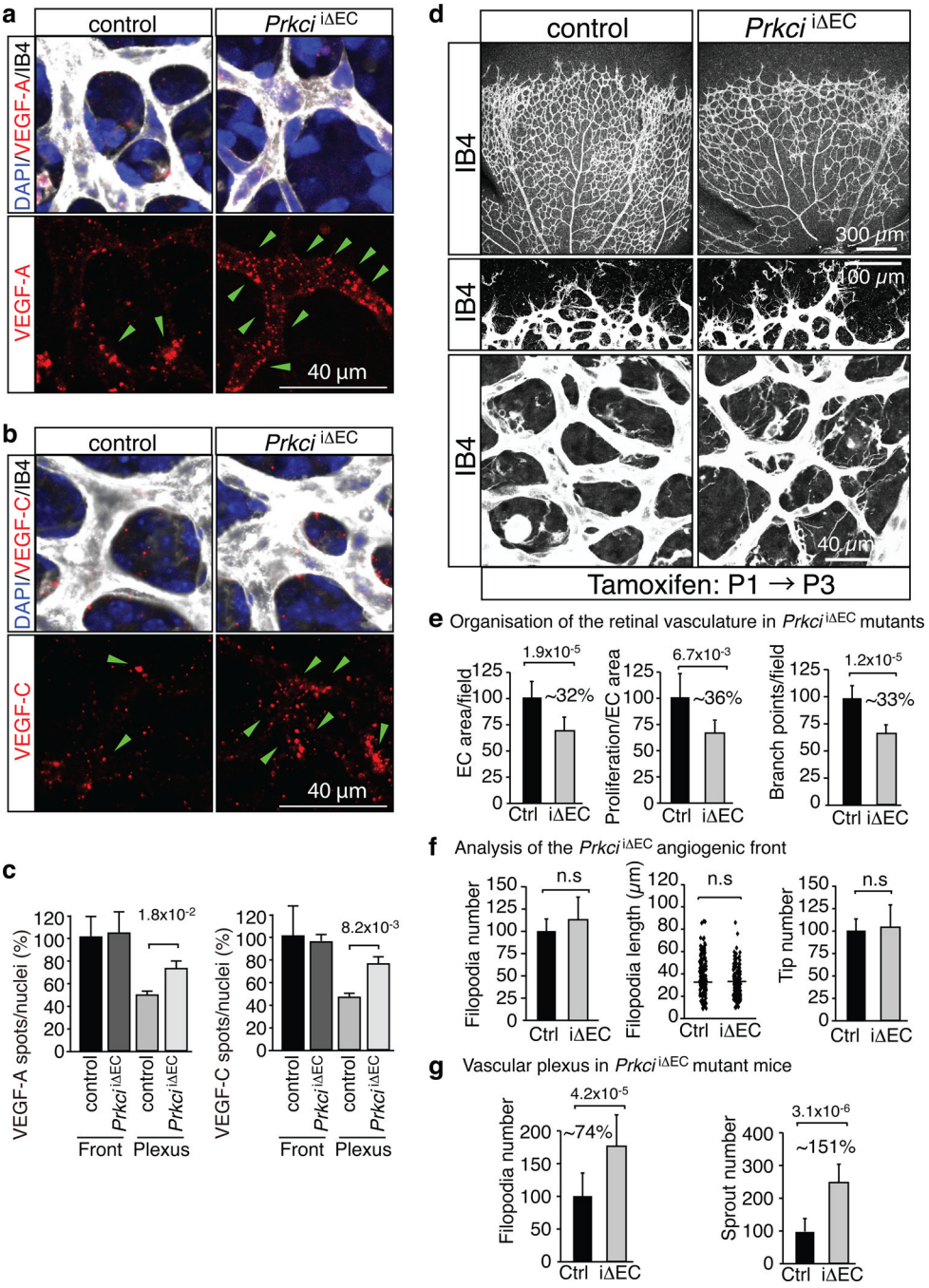

Figure 7. Increased VEGF uptake and sprouting in the *Prkci*$^{i\Delta EC}$ central retina

a, b, VEGF-A (red, **a**) or VEGF-C (**b**) uptake in the *Prkci*$^{i\Delta EC}$ central plexus. Green arrowheads indicate ligand spots. Cell nuclei, DAPI (blue); ECs, Isolectin B4 (IB4, white). **c**, Statistical analysis of internalised VEGFs as shown in (**a**) and (**b**). Data represent the means±s.d. of 6 independent experiments. P values, two-tailed Student's t-test. **d**, Phenotype of the Isolectin B4-stained (IB4) P6 *Prkci*$^{i\Delta EC}$ retinal vasculature. Higher magnification of the angiogenic front (middle) and central plexus (bottom) are shown. **e–g**, Quantitation of vessels branch points, EC area and proliferation (**e**, n=3), the number and length of filopodia and the number of distal sprout tips at the angiogenic front (**f**, n=6),

and the number of ectopic sprouts and filopodia (**g**, n=6) in the central retina of *Prkci* mutants (iΔEC) compared to control (Ctrl) retinas. Data represent the means±s.d. P values, two-tailed Student's t-test

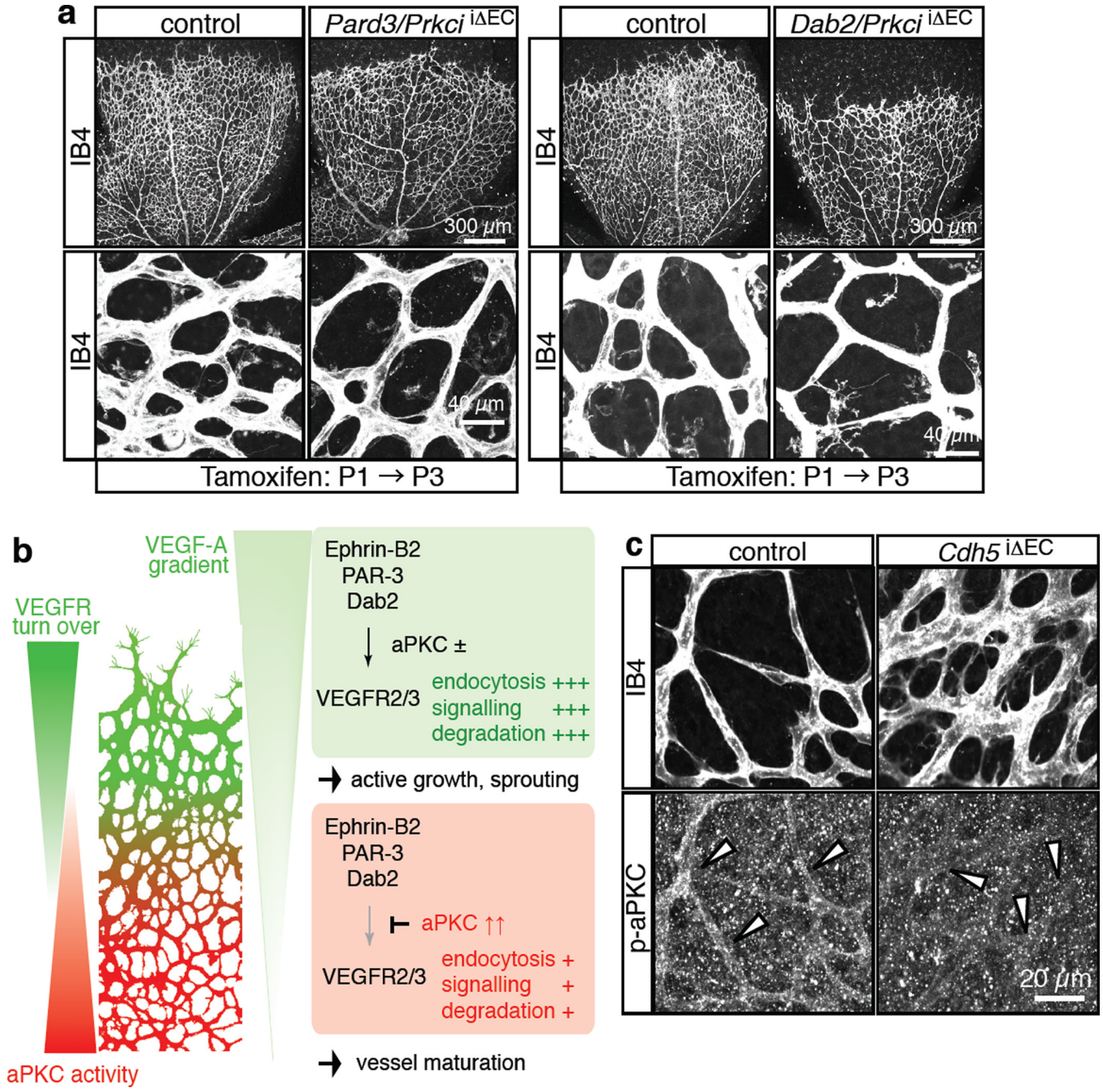

Figure 8. Schematic depiction of key findings

a, Absence of ectopic sprouting and filopodia in the central retina of *Pard3/Prkci*$^{i\Delta EC}$ (left) or *Dab2/Prkci*$^{i\Delta EC}$ (right) double mutant mice (compare to lower panels to equivalent regions shown in Fig. 7d). ECs, Isolectin B4 (IB4, white).

b, VEGF receptor turnover (i.e. internalisation, degradation and new synthesis) is highest in vessel sprouts at the angiogenic front compared to the more mature central vessel plexus. This behaviour is not solely controlled by the VEGF-A gradient, but also intrinsic properties of ECs. VEGF receptor internalisation and certain downstream signalling processes are controlled by the transmembrane protein ephrin-B2 and its interaction partners PAR-3 and Dab2. Abundant active (phosphorylated) aPKC in the central retina antagonizes VEGF

receptor internalisation by phosphorylating the Dab2 (cargo-binding) PTB domain. This contributes to regional differences in VEGF receptor turnover and VEGF ligand internalisation. We propose that regionally distinct behaviours of ECs in the growing vasculature are modulated by spatially regulated endocytosis.

c, Anti-phospho-aPKC (p-aPKC, Thr403; Cell Signaling, lot 8) and Isolectin B4 (IB4) staining of P6 control and $^{Cdh5i\Delta EC}$ retinal vessels.